Local and Nonlocal Contributions to the Linear Spectroscopy of Light-Harvesting Antenna Systems

M. H. C. Koolhaas,[†] G. van der Zwan,*,[†] and R. van Grondelle[‡]

Department of Analytical Chemistry and Applied Spectroscopy, and Department of Biophysics and
Physics of Complex Systems, Faculty of Sciences, Vrije Universiteit, De Boelelaan 1081,
1081 hv Amsterdam, The Netherlands

Received: June 3, 1999; In Final Form: February 3, 2000

In this paper the circular dichroism and absorption spectra of the LH2 complex of *Rhodopseudomonas acidophila*, for which the atomic structure is known, are analyzed. We show that an analysis based on the distribution of the excitations in real space, and their correlations, to unravel the relation between the atomic structure of the light-harvesting complex and its excitonic properties, is particularly successful. Starting from molecular expressions for the linear susceptibility, we demonstrate that linear spectra can be viewed as originating from the product of coherence correlation functions and geometric structure factors. Effects of homogeneous and inhomogeneous broadening can be incorporated in a natural way and lead to a definition of exciton length as the distance over which coherence correlation functions decay.

1. Introduction

In photosynthesis two fundamental processes play a key role in converting solar energy into free chemical energy: energy absorption and energy transfer in light-harvesting (LH) complexes and charge separation in the reaction center (RC).[1,2] Though the elucidation of the crystal structure of LH2 of *Rhodopseudomonas acidophila* by Cogdell and co-workers[3] was a major breakthrough, spectroscopic properties of LH2 and the energy-transfer mechanism are still not fully understood (see, for example, Pullerits and Sundström[4] and Fleming and Van Grondelle[5] for a discussion).

Several attempts were made recently to obtain the linear spectroscopic properties of LH2 of *Rps. acidophila* from the geometric structure. Thus, Sauer[6] successfully calculated the absorption (OD) spectrum from the LH2 structure in combination with extended charge distributions on the pigments. Calculation of the circular dichroism (CD) spectrum proved to be more difficult, as a consequence of the canceling effects due to line-broadening mechanisms. Koolhaas et al.[7] gave a similar analysis, albeit with point transition dipole moments on the pigments, and they came to the conclusion that the aforementioned canceling effects were less important when an energy difference between the α- and β-bound chromophores was introduced. This led to a prediction of both the OD and CD spectrum and an interpretation of the origin of the red-shifted zero crossing of the CD spectrum with respect to the absorption maximum. It was concluded that interactions among BChl's over more than half the ring had to be taken into account in order to explain this crucial feature. Some of the assumptions in the above-mentioned papers were confirmed by Alden et al.[8] who showed, based on ab initio calculations of the BChl's only, one of which is slightly bent, that indeed an energy difference between α- and β-bound pigments can occur. An additional reason for the difference in energy can be found in the

dissimilarity of the protein environment. In particular it is thought that the 2-acetyl carbonyl H-bonds between BChl*a* and the α-Tyr-44 and α-Tyr-45 can give rise to a considerable red shift in the absorption maximum.[9,10] Another result of the calculations done by Alden et al.[8] is that the effect of the charge-transfer states on the steady-state linear spectroscopy is negligible.

A recent study[11] of a B800-free LH2 complex of *Rhodobacter sphaeroides* led to an accurate set of parameters that quantitatively explained the absorption and CD features of the B850-ring. The geometric structure of this ring, with slightly different α- and β-pigments, gives rise to so-called Davidov splitting, which leads to weak spectroscopic effects in the 770−800 nm region. These contributions were indeed observed and could hence be used to obtain a direct estimate of the excitonic interaction between neighboring pigments, which was determined to be approximately 300 cm^{-1} in *Rb. sphaeroides*.

In this paper we present a detailed analysis of the linear spectroscopic properties of the highly symmetric rings of pigments. These include OD, CD, and also linear dichroism (LD) on oriented samples. We aim at understanding detailed features of the spectra, which include peak positions and relative magnitudes, zero crossings of the CD spectra, and positions of change in the LD spectra.

This paper consists of two distinct parts, which taken together give a general description of the linear spectroscopic features of ring-shaped antenna complexes, in the sense that the spectra can be used to make predictions about the structure of LH antennae complex and vice versa, and the structure can be used to calculate the spectra.

The first part concerns the description of LH complexes as interacting rings. As an example we consider LH2 of *Rps. acidophila*. The crystal structure of this complex was obtained with a resolution of 2.5 Å at room temperature[3] and has a C_9 symmetry axis. It shows a highly organized arrangement of two concentric rings of polypeptides, the α-polypeptides inside and the β-polypeptides outside, and bound to these two vertically displaced rings of bacteriochlorophyll *a* (BChl*a*). One ring

---

* Corresponding author.
† Department of Analytical Chemistry and Applied Spectroscopy.
‡ Department of Biophysics and Physics of Complex Systems.

comprising nine BChl*a*'s is called B800 since its main absorption is around 800 nm. The other ring (B850) consists of 18 BChl*a*'s, sandwiched between the α- and *β*-polypeptide rings, and absorbs mainly around 870 nm at 4 K and 855 nm at room temperature. In fact this B850 ring itself can be viewed as two interlocking rings, namely, a ring of α-bound chromophores and a ring of *β*-bound chromophores. It can therefore be viewed as a ring of dimers.[12] However, in this paper we will develop a description in which the B850 ring can best be considered as a dimer of rings. The coupling between the rings can be expressed analytically in the coupling between all monomers, not just nearest neighbors. This picture leads to an easy extension to more complex cases. After all, even in LH2 the BChl*a*'s are not the only rings; the carotenoids in the structure form yet another ring, and other transitions such as the Q_x transition of the monomers can be resolved separately first and subsequently be coupled to the Q_y ring. This leads to the view that the OD, CD, and LD features can be understood as resulting from properties of the ring as a whole, which in turn derive directly from the position and orientation of the monomers in the ring.

So far we considered the LH2 system as an ideal, unperturbed set of rings. In reality external perturbations (inhomgeneities) destroy the ideal ring structure. However, we show that, on average, the excitonic structure described above remains intact and that linear spectroscopic features can be understood as probes of this structure. Therefore, in the second part of this paper, we calculate the first-order response of the antenna system to an external light field, based on the so-called real space description of density matrices developed by Mukamel et al.[13,14] It is shown that the linear susceptibility can be broken down into two parts: a structural part, independent of position and shape of absorption lines but dependent on the geometry of the ring, and frequency-dependent coherence correlation functions of which the specific form is related to homogeneous and inhomogeneous broadening mechanisms. We show that the spectra can be viewed as the result of probing these correlation functions by different structure functions. For isotropic samples there are three structure functions,[15] two of which can be measured independently, the first one related to OD, the second to CD. It will be shown that these probe the coherence correlations of different parts of the ring: OD mainly nearest neighbors, CD mainly pigments a quarter of the ring apart. For oriented samples there is in addition LD, which gives all pigments equal weight.

The description presented in this paper also sheds some light on the problem of exciton length, the number of pigments over which the excitation is delocalized, and the related property of spectroscopic unit, the minimal number of coupled pigments needed to explain spectroscopic features. The size of the exciton was interpreted as the size of a spectroscopic unit as was pointed out in theoretical studies on steady-state spectroscopy,[6,7,16] in which the spectroscopic unit was defined as a subunit of the LH2 system, large enough to explain all linear spectroscopic properties. A correct simulation of the CD spectrum requires a spectroscopic unit of at least half the size of the ring. Estimates of the size of the exciton based on various experiments vary between a dimer and at least half the LH2 ring.[17−25] The time-dependent properties of the antenna systems are interpreted in terms of a small hopping exciton: excitation of the system rapidly leads to a localized quasi particle, which by a random walk hops to neighboring sites[26−30] and eventually to the special pair of the RC. The localization is thought to be the result of energy disorder and/or electron−phonon coupling.[31,32]

The real space description, however, will naturally lead to a

definition of the exciton length based on the correlation length, which is the determining factor in interpreting spectra. This model is very useful because it is applicable to localized and delocalized excitons. We will show that OD spectra are determined mainly by short-range correlations, whereas in LH1 and LH2 longer range correlations are important in explaining CD spectra. Although in this paper we limit ourselves to a simple model for the dynamics of the excitonic states (they all decay to the ground state with the same relaxation rate), we show that the effects of diagonal disorder, which is static, and homogeneous line width, which is of a dynamical nature, on the size of the exciton are indeed similar. One of the results presented in this paper is that inhomogeneous broadening based on diagonal disorder does not fully destroy the averaged excitonic structure of the rings. Simply stated we can say that with the given parameters on the average the ring displays the original C_9 symmetry and that the coherence correlation functions clearly exhibit features related to this symmetry. Phase relations remain valid, although amplitudes of longer ranged coherences decay. Thus diagonal disorder of the magnitude considered in this paper does not lead to complete localization.

It is possible to incorporate more sophisticated models for the time-dependent properties of the system, such as decay to the lowest excitonic state within the exciton manifold. However, these models have minor effects on the steady-state spectroscopic properties described in this paper.

The organization of this paper is as follows. In the next section we will give a brief review of the diagonalization of the Hamiltonian for ring systems and show that rings of dimers can also be interpreted as dimers of rings, with the simplification that a full ring only consists of two levels, one doubly degenerate, and that only excitons with the same wave number couple. The subsequent section is devoted to the real space description of the density matrix as applied to ring systems. The separation into a structural and a frequency-dependent part is effected, and the properties of these two parts are further elucidated in separate sections.

2. Hamiltonian of the System and Excitonic States

We begin by considering a ring of N excitonically coupled monomers with C_N symmetry. Although it is possible to get the full excitonic structure, including multiple excitations, for such a system, this is a rather involved procedure, which is only useful when nonlinear forms of spectroscopy are used to probe the system. The full solution will be presented elsewhere; here we restrict ourselves to singly excited states, which is sufficient for the calculation of the linear susceptibility $\chi^{(1)}$.

The Hamiltonian of the system with excitonic interaction is given by

$$ H = \epsilon \sum_{n=1}^{N} |n\rangle \langle n| + \frac{1}{2} \sum_{n,m=1}^{N} {}' V_{nm} [|n\rangle \langle m| + |m\rangle \langle n|] \quad (1) $$

where N is the number of pigments and with V_{nm} the coupling strength between monomer n and m.

We note that owing to the symmetry of the system V_{nm} only depends on $|n - m|$ so that we can write $V_{nm} \equiv V_{|n-m|}$ and $V_{N-m} = V_m$. These properties allow the Hamiltonian to be diagonalized by the well-known transformation to excitonic states

$$ |\psi_k\rangle = \frac{1}{\sqrt{N}} \sum_{n=1}^{N} e^{2\pi ink/N} |n\rangle \quad (2) $$

Contributions to the Linear Spectroscopy of LH2

J. Phys. Chem. B, Vol. 104, No. 18, 2000 **4491**

with the result

$$H = \sum_{k=0}^{N-1} E_k |\psi_k\rangle \langle \psi_k| \qquad (3)$$

where

$$E_k = \epsilon + \tilde{V}(k) \equiv \epsilon + \sum_{n=1}^{N} V_n e^{2\pi ikn/N} \qquad (4)$$

For the Q_y transitions in the α- and β-ring the nearest-neighbor interaction is negative owing to the almost tangential orientation of the transition dipoles, which makes E_N the lowest energy, and the next level up is $E_1 = E_{N-1}$.

It is obvious from eq 4 that $E_{N-k} = E_k$, so that every level except $k = 0$ and (possibly) $k = N/2$ is degenerate. More important is that the transition moments to the excited states are all zero, except those to level $k = 0$, and those to the (degenerate) levels $k = 1$ and $k = N - 1$. As is well-known, the transition moment to the lowest excited state is small and in the direction perpendicular to the B850 plane, and the transition moments to the next excited state are in the aggregate plane and much larger, approximately $\sqrt{N}$ times the monomer moment.

For the explanation of CD, it is useful to introduce magnetic transition moments to the excitonic states, $\vec{m}_k = \sum_{n=1}^{N} \vec{r}_n \times \vec{\mu} e^{-2\pi ikn/N}$, which also transform as vectors under proper rotations and consequently have properties similar to those of the electric dipole moments. In contrast to the electric moments for B850 of LH2, the magnetic moment has a large component in the aggregate z direction, since both $\vec{\mu}_n$ and $\vec{r}_n$ are almost in the xy-plane of the ring.

For a ring of dimers, or a ring of three-level systems (if we also take the Q_x transition into account), the above description is easily extended. In fact the single-exciton level structures of these two systems are equivalent, since we can always diagonalize the dimer first to get a three-level system. For LH2 the dimers are actually a better starting point than the monomers, since the α- and β-bound BChl$a$'s do not have the same orientation, so the B850 ring of the LH2 has no C_{18} symmetry anyway. In addition this allows us to give different site energies to the α- and β-bound chromophores. The same is true for LH1, a 16-fold symmetric ring of B820 dimers.[33,34]

For a ring of N dimers we introduce the basis one-exciton states $|n, \nu\rangle$, where n runs from 1 to N, denoting the position of the dimer, and ν can be 1 (α) or 2 (β), denoting the monomers within the dimer; see Figure 1.

The dimer Hamiltonian is then given by

$$H_n = \sum_{\nu=1}^{2} \epsilon_\nu |n, \nu\rangle \langle n, \nu| + \frac{1}{2} \sum_{\nu,\nu'=1}^{2} {}' V_{n\nu,n\nu'} [|n, \nu\rangle \langle n, \nu'| +$$
$$|n, \nu'\rangle \langle n, \nu|] \quad (5)$$

where $V_{n\nu,n\nu'}$ is the interaction between pigments within a dimer.

The Hamiltonian of the ring then becomes

$$H = \sum_{n=1}^{N} \sum_{\nu=1}^{2} \epsilon_\nu |n, \nu\rangle \langle n, \nu| + \frac{1}{2} \sum_{n,m=1}^{N} \frac{{}^{\nu,\nu'=1}}{2} {}' V_{n\nu,m\nu'} [|n\nu\rangle$$
$$\langle m\nu'| + |m, \nu'\rangle \langle n, \nu|] \quad (6)$$

and the transformation to excitonic states corresponding to eq 3 is
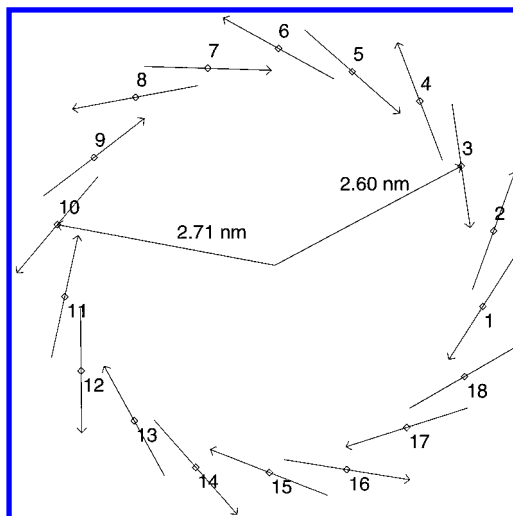

Figure 1. Positions and orientations of the transition dipole moments in the plane of the B850 ring in LH2 of *Rps. acidophila*. Not shown is the slight deviation (5−7°) in the positive z-direction of both the α- and β-transition dipole moments, and the small z-components of the Mg atoms (±0.02 nm). Throughout this paper we use the convention that odd-numbered atoms correspond to α-bound pigments and even-numbered atoms to β-bound pigments. In the unit cell notation ($n\nu$) used in sections 2 and 3, the (n1)-pigment is an α-chromophore located at position $2n - 1$, and the (n2)-pigment a β-chromophore at position $2n$.

$$|\psi_k, \nu\rangle = \frac{1}{\sqrt{N}} \sum_{n=1}^{N} e^{2\pi ikn/N} |n, \nu\rangle \qquad (7)$$

This transformation now leads to the following Hamiltonian in the exciton basis

$$H = \sum_{k=0}^{N-1} \sum_{\nu,\nu'=1}^{2} (\epsilon_\nu \delta_{\nu,\nu'} + \tilde{V}_{\nu\nu'}(k)) |\psi_k, \nu\rangle \langle \psi_k, \nu'| \qquad (8)$$

with

$$\tilde{V}_{\nu\nu'}(k) = \sum_{n=1}^{N} V_{1\nu,n\nu'} e^{2\pi i(n-1)k/N} \qquad (9)$$

Again we see that $\tilde{V}_{\nu\nu'}(k) = \tilde{V}_{\nu'\nu}^{*}(k)$ and $\tilde{V}_{\nu\nu'}(N - k) = \tilde{V}_{\nu\nu'}(k)$, so that every level, except for $k = N$ and, for N even, $k = N/2$, is still degenerate. For a complete discussion regarding the group theoretical representations of the C_9 group and its consequences for the spectroscopy of antenna systems, see ref 35.

Thus, for every value of k we have reduced the problem to diagonalization of a 2×2 matrix, which is fully equivalent to the problem of two interacting monomers in a dimer, where a further simplification occurs since the dipole moments belonging to the "monomers" $|\psi_k, \nu\rangle$ are parallel. This allows us to give a picture of the interaction between the rings, which we will frequently use in the subsequent sections to give insight into the origin of spectral features. As an example we take the $k = 0$ level. The $\tilde{V}_{12}(0)$ interaction is dominated by the $V_{11,12}$ term, which for LH2 is positive. From the results given in the Appendix, it can be inferred that if the interaction energy is positive, the transition moments add in the high-energy state, (with the proper coefficients) and are subtracted in the lowest energy state. Therefore, in LH2 the highest excitonic B850 state (around 789 nm) will have considerably more z-character then the lowest excitonic state (around 859 nm). The total energy

TABLE 1: Values of Physical Parameters Used in the Simulations[a]

quantity	value
Q_y transition moment	6.3 D
α−α interaction: $V_{1\alpha,2\alpha}$	-52 cm^{-1}
α−β interaction: $V_{1\alpha,1\beta}$	396 cm^{-1}
β−α interaction: $V_{1\beta,2\alpha}$	300 cm^{-1}
β−β interaction: $V_{1\beta,2\beta}$	-36 cm^{-1}
relative dielectric constant ε	1.7
α-site energy	12 300 cm^{-1} (813 nm)
β-site energy	12 000 cm^{-1} (833 nm)

[a] The interaction energies were calculated directly from the structure, with the given value of the transition dipole moment. Values given are for ε = 1. The relative dielectric constant and site energies given in this table give good fits of the absorption and CD spectra.

splitting is approximately equal to $2\tilde{V}_{12}(0)$, since $\tilde{V}_{11}(0) \approx \tilde{V}_{22}(0)$. This also determines the total width of the exciton manifold.

For completeness, we give in Table 1 a list of values of the interaction energies, site energies, and other relevant parameters used in the simulations later in this paper.

Before presenting a more detailed analysis of spectral features, we now first turn to the nonlocal description of the density matrix, which allows us to discuss structural issues, such as the ones given in this section, and problems related to homogeneous and inhomogeneous broadening separately.

3. Real Space Formulation of the Linear Susceptibility

In a real space, or nonlocal, formulation of the susceptibilities, it is necessary to keep track of the positions of the transition dipole moments of the system. This allows us to take into account the variation of the electric field over the pigments in the system. This is important in understanding excitonic CD spectrosopy and energy transfer in extended systems. An extensive treatment and application to naphthalene was given in ref 14, and here we restrict ourselves to the linear susceptibilities and apply it to the ring systems discussed in the previous sections. A direct application of the theory (ref 13, Chapter 5) to the system at hand gives for the linear susceptibility in the coordinate frame of the ring

$$\chi(\vec{r}, \vec{r}', \omega) = -\frac{1}{\hbar} \sum_{k,\gamma} \sum_{n,\nu} \sum_{m,\nu'} C_{n\nu}^{k\gamma} C_{m\nu'}^{k\gamma*} \, G(\omega_0 - \omega_{k\gamma}) \, \vec{\mu}_{n\nu} \vec{\mu}_{m\nu'} \, \delta(\vec{r} - \vec{r}_{n\nu}) \, \delta(\vec{r}' - \vec{r}_{m\nu'}) \quad (10)$$

where, as in the previous section, Latin indices indicate unit cells, while the indices ν and ν' indicate monomers within a dimer. The index γ now indicates the highest ($\gamma = 1$) and lowest ($\gamma = 2$) energy level within the excitonic state k, due to Davidov splitting.

In this expression $\vec{\mu}_{n\nu}$ are the transition moments and $\vec{r}_{n\nu}$ the positions of the chromophores, as introduced in the previous section, and the coefficients $C_{n\nu}^{k\gamma}$ are given for the perfect ring in the Appendix. The frequencies $\omega_{k\gamma}$ are equal to the energy eigenvalues for the system divided by $\hbar$: $\omega_{k\gamma} = \epsilon_\gamma(k)/\hbar$; see the Appendix. The Green functions $G(\omega_0 - \omega_{k\gamma})$, which reflect the dynamical behavior of the system, depend on these frequencies as well as on the model for homogeneous broadening; in this work Gaussian profiles are used to calculate the high-temperature spectra (ref 13, Chapter 8). It is clear from eq 10 that the susceptibility now depends on the positions $\vec{r}$ and $\vec{r}'$, so that an external field acting at position $\vec{r}$ can generate polarization at a different position $\vec{r}'$.

The absorption intensity is now given by

$$I(\omega) = \frac{\omega}{\pi} \int d\vec{r} \int d\vec{r}' \, \vec{E}(\vec{r}, \omega) \cdot \text{Im} \, [\chi(\vec{r}, \vec{r}', \omega)] \cdot \vec{E}(\vec{r}', \omega) \quad (11)$$

The result of isotropic averaging up to lowest order in $k_0 L$, where k_0 is the wavenumber of the incident light and L the extension of the system, is[15,16]

$$\frac{I(\omega_0)}{\int dt \, E_0^2(t)} = -\frac{\omega_0}{3\pi\hbar} \sum_{k,\gamma} G(\omega_0 - \omega_{k\gamma}) \sum_{n,\nu;m,\nu'} C_{n\nu}^{k\gamma} C_{m\nu'}^{k\gamma*}$$
$$(\vec{\mu}_{n\nu} \cdot \vec{\mu}_{m\nu'} - 2(\vec{\mu}_{n\nu} \times \vec{\mu}_{m\nu'}) \cdot (\vec{r}_{n\nu} - \vec{r}_{m\nu'}) \, k_0 \sin \phi) \quad (12)$$

where ω_0 is the frequency of the incident light. To obtain this expression we also assumed that the light field can be represented by plane waves with slowly varying amplitude $\vec{E}_0(t)$

$$\vec{E}(\vec{r}, t) = \vec{E}_0(t) e^{i\vec{k}_0 \cdot \vec{r} - i\omega_0 t} + \vec{E}_0^*(t) e^{-i\vec{k}_0 \cdot \vec{r} + i\omega_0 t} \quad (13)$$

where $\vec{E}_0(t)$ is furthermore given by

$$\vec{E}_0(t) = E_0(t) \, [\vec{\epsilon} + e^{i\phi} \vec{\epsilon}'] \quad (14)$$

In this last equation $\vec{\epsilon}$ and $\vec{\epsilon}'$ are two orthogonal unit vectors in the plane perpendicular to the direction of propagation $\vec{k}_0$ of the light. Polarization properties depend on the value of ϕ (ref 36, Chapter 8).

We note that all optical activity of the sample originates from the contribution of the second term in parentheses in eq 12 to the absorption intensity. For linearly polarized light $\phi = 0$, and the second term does not contribute.

Homogeneous and Inhomogeneous Broadening. The effects of homogeneous and inhomogeneous broadening must be incorporated into eq 12. For homogeneous broadening we use a simple model. At high temperatures the rapid fluctuations of the modes of the surrounding medium that couple to electronic transitions give rise to Gaussian line shapes.[13] Thus we assume that the Green functions G have the following frequency dependence

$$G(\omega_0 - \omega_{k\gamma}) = \frac{1}{\sigma\sqrt{2\pi}} e^{-(\omega_0 - \omega_{k\gamma})^2/2\sigma^2} \quad (15)$$

for each of the excitonic states. The homogeneous line width σ, which depends on the temperature and the Stokes shift, is assumed to be the same for all states. This assumption is probably not valid for the lowest excitonic level; it is generally assumed that this state has a considerably longer lifetime than the other excitonic states[18,37,38] at least at low temperatures. It is of course possible to incorporate more sophisticated models for the exciton−phonon interaction or other relaxation pathways to use other excitonic homogeneous line shapes in eq 15. In general the homogeneous line width is larger than the energy difference between the excitonic levels, especially for the lower states where the levels are close together.

The origin of inhomogeneous broadening is static disorder, and we assume that its main effect is on the ground-state energy of the monomers. This so-called diagonal disorder can then be modeled by giving each of the monomer levels a random energy contribution, chosen from a Gaussian distribution with standard deviation Δ. This means in fact that we add a random Hamiltonian H_r to eq 5 of the form

Contributions to the Linear Spectroscopy of LH2

J. Phys. Chem. B, Vol. 104, No. 18, 2000 **4493**

$$H_r' = \sum_{n,\nu} \lambda_{n\nu} |n\nu\rangle \langle n\nu| \tag{16}$$

and numerically diagonalize the resulting system. This has two effects: the eigenfrequencies $\omega_{k\gamma}$ and the coefficients $C_{n\nu}^{k\gamma}$ become dependent on the parameter set $\{\lambda\}$. Although it is possible to keep the $|\psi_k, \gamma\rangle$ states as the basis and to induce coupling between these electronic states as a result of the disorder,[35] for large disorder the excitonic structure becomes mixed, and the nature of these states is lost. In the following we therefore leave out the index γ, and let k run over all the states resulting from the diagonalization of $H + H_r'$. Note that the index k now runs from 0 to $2N - 1$.

Equation 12 then becomes an average over all possible realizations

$$I(\omega_0) \propto \sum_{n\alpha;m\beta} F_{n\nu,m\nu'}(\omega_0) [\vec{\mu}_{n\nu} \cdot \vec{\mu}_{m\nu'} - 2(\vec{\mu}_{n\nu} \times \vec{\mu}_{m\nu'}) \cdot$$

$$(\vec{r}_{n\nu} - \vec{r}_{m\nu'}) k_0 \sin \phi] \tag{17}$$

with coherence correlation functions

$$F_{n\nu,m\nu'}(\omega) = \sum_{k=0}^{2N-1} \langle G(\omega - \omega_k) C_{n\nu}^k C_{m\nu'}^{k*} \rangle \tag{18}$$

where $\langle \cdots \rangle$ is an average over the diagonal disorder. These functions are a measure of the nonlocality of the system, in other words, the correlation between an excitation, or coherence, of pigment $n\nu$ at position $\vec{r}_{n\nu}$ and another one at $\vec{r}_{m\nu'}$. These correlation functions can be probed by various spectrocopic methods.

The correlation functions, $F_{n\nu,m\nu'}(\omega)$, are the measurable quantities in combination with a probe and structure-dependent factor. They are obtained by calculating eigenvalues ω_k and coefficients $C_{n\nu}^k$ and summing over all excitonic states. This latter point is rather crucial: we do not keep track of each excitonic state this way, but consider the energy (frequency) at which it occurs as more relevant. After all, experimentally systems are probed at a given frequency, and in general one does not know whether the state of an individual aggregate is the lowest state or some higher excitonic state, especially when there is considerable overlap between the excitonic states, i.e., when $\Delta/V > 1$ and $\sigma/V \approx 1$.

Two limiting cases, small and large homogeneous/inhomogeneous width, give rise to simpler expressions. For small Δ, i.e., $\Delta/V \ll 1$, we can study the effect of the disorder on the exciton functions in terms of the unperturbed excitonic states.[35] The unperturbed Hamiltonian is diagonal in this representation, and the contribution to the random Hamiltonian has two effects: all diagonal elements, the eigenenergies, get an extra contribution $\{1/(2N)\}\sum_i \lambda_i$, and all nondiagonal elements also become nonzero, introducing a coupling between the excitonic states. The diagonal part does not influence the coefficients, and the off-diagonal part has only second-order effects. We therefore assume that we can make the following approximation for the average over all inhomogeneities if the disorder is small:

$$\langle G(\omega_0 - \omega_k) C_{n\nu}^k C_{m\nu'}^k \rangle \approx \langle G(\omega_0 - \omega_k) \rangle \langle C_{n\nu}^k C_{m\nu'}^k \rangle \tag{19}$$

Furthermore, the dominant effect on the frequency is a shift: $\omega_k \to \omega_k + \{1/(2N)\}\sum_i \lambda_i$. Since G is a Gaussian, this means that upon averaging, with a Gaussian distribution for all λ_i, this function becomes

$$\langle G(\omega_0 - \omega_k) \rangle = \frac{1}{\sigma\sqrt{2\pi}} \langle e^{-(\omega_0 - \omega_k - (1/N)\sum_i \lambda_i)^2/2\sigma^2} \rangle =$$

$$\frac{1}{\sigma'\sqrt{2\pi}} e^{-(\omega_0 - \omega_k)^2/2\sigma'^2} \tag{20}$$

with

$$\sigma'^2 = \sigma^2 + \frac{\Delta^2}{N'} \tag{21}$$

Effectively this leads to a change in the homogeneous broadening parameter. Since the value of σ is hard to determine, we may as well take σ' as the parameter to fit the spectra. The result is that in this limit that we get slightly broadened lines at the unperturbed frequencies; see Figure 2a.

The value of N' is *not* the same for all lines. For the two outer levels, which are nondegenerate, its value equals $2N$, the number of pigments in the ring; for all other (degenerate) states it is equal to N.

In Figure 2b we show the results of the correlation functions for slightly larger σ', large enough to cause some overlap of the excitonic states at the band edge, where they are close together, but small enough to leave the inner excitonic levels unperturbed. It is clear that at the band edges the coherence correlations have already decayed in space, and no spatial decay is observed for intermediate exciton levels. Since the total width of the exciton manifold is determined by the nearest-neighbor interaction energy, cf. section 2, and the total number of levels by the number of monomers in the ring, and, owing to exchange narrowing the overlap scales with $\Delta/\sqrt{N}$, the decay of correlation functions is somewhat faster for larger ring sizes.

For large σ and/or Δ, i.e., much larger than any excitonic energy difference, we can neglect the ω_k dependence in G and approximate the k-dependent part of eq 21 as follows:

$$\sum_k \langle G(\omega_0 - \omega_k) C_{n\nu}^k C_{m\nu'}^k \rangle \approx G(\omega_0) \sum_k \langle C_{n\nu}^k C_{m\nu'}^k \rangle =$$

$$G(\omega_0) \delta_{n\nu,m\nu'} \tag{22}$$

So, in this case, the correlation functions are effectively reduced to δ functions; in other words, the monomers are completely uncorrelated.

In all intermediate cases the exciton length could be related to the range over which $F_{n\nu,m\nu'}(\omega)$ are nonzero. From the above limiting cases we can infer that for small homogeneous and inhomogeneous broadening this range is effectively the whole ring, whereas for very large inhomogeneities all correlations between neighboring chromophores vanish; cf. eq 22. For antenna systems we are clearly in the intermediate regime: both the homogeneous and the inhomogeneous line width, σ and Δ, are larger than the energy separation between excitonic states but considerably smaller than the width of the complete excitonic manifold.

4. Coherence Correlations and Exciton Size

In this section we will show how the functions $F_{n\nu,m\nu'}(\omega)$ can be used to define an exciton length that on hand can be used as a measure of contributions to an excitonic state and on the other hand can also be used directly in the explanation of spectroscopic features. We concentrate on the functions $F_{n\nu,m\nu'}(\omega)$ for ring systems, which leads to the simplification that these functions only depend on $|n\nu - m\nu'|$.

The current paradigm in excitonic theory of disordered systems is illustrated in Figure 3a. For a particular realization
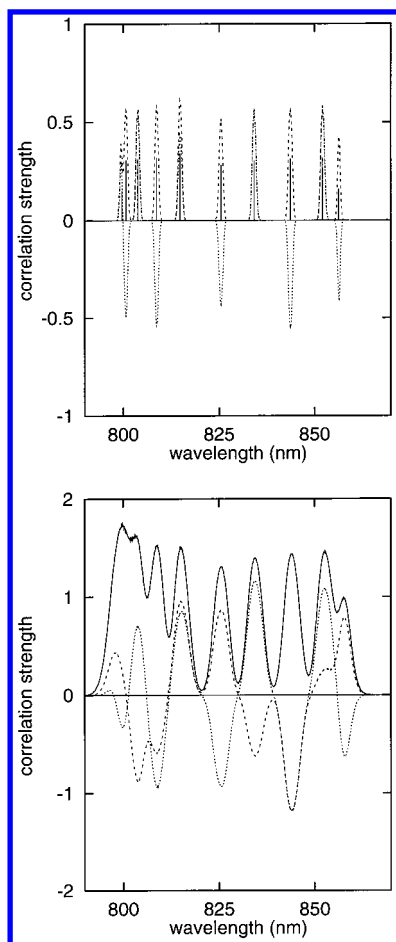
Figure 2. (a, top) Autocorrelation function $F_{11,11}(\omega)$(---) and opposite side of the ring coherence correlation function $F_{11,51}(\omega)$(···) for small diagonal disorder, $\Delta = 20$ cm^{-1}, and zero homogeneous broadening. For positive amplitude the functions overlap completely. Also shown is the first function for zero disorder (solid lines), which gives the positions of the excitonic states as a function of the wavelength. There is some minor overlap between the two highest excitonic states, but overall there is no noticeable decay in the correlations. (b, bottom) Autocorrelation function $F_{11,11}(\omega)$(—) and coherence correlation functions $F_{11,22}(\omega)$(---) and $F_{11,51}(\omega)$(···), but now for $\Delta = 80$ cm^{-1} and zero homogeneous width. There is considerable overlap at the band edges, leading to smaller magnitude of the coherence correlation, whereas in the middle, where the average distance between excitonic levels is approximately 100 cm^{-1}, there is no overlap and consequently no decay of the coherence correlation.

from a random distribution with $\Delta/V \approx 2$, where V is the average nearest-neighbor interaction, the excitonic states are calculated, and from these we calculate the contribution of each of the pigments, that is, $|C_n^k|^2$. The figure shows the result of this calculation for the two lowest states, $k = 0, 1$, for this particular realization. This picture is then used to suggest that two to three pigments "participate" in these excitonic states.

There are a number of obvious limitations to this picture. The first is that there is no direct connection between the transition dipole moment of the excitonic state and the populations in Figure 3a. In fact calculations for these states show that, although they do not look the same, their transition dipole moments have similar sizes. The reason is that the populations of the BChl's do not play a dominant role in the calculation of transition dipoles; coherences (i.e., the off-diagonal elements of the density matrix) of the pigments do, but they do not appear in this view. In fact populations can play a role in selected nonlinear spectroscopic measurements, for instance, fluorescence
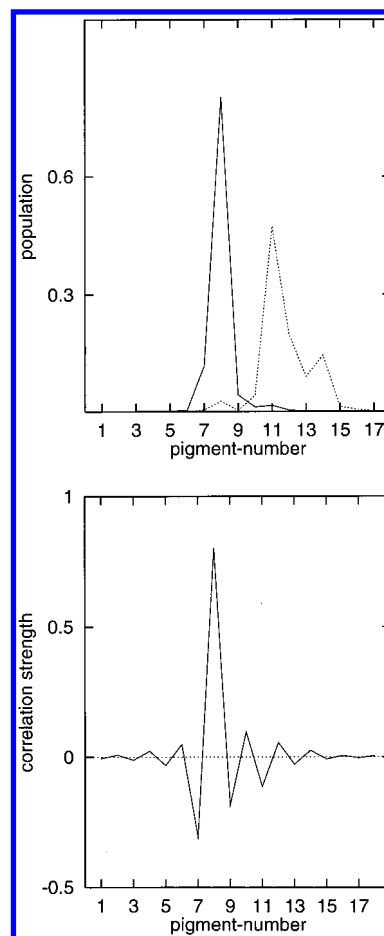

Figure 3. (a, top) Probability that pigment n is excited, $|C_n^k|^2$, in the lowest exciton level ($k = 0$, solid line) and the next to lowest ($k = 1$, dotted line) for a particular realization, from a random distribution with $\Delta/V \approx 2$, of excitation energies of the chromophores in the B850 band. Their transition energies correspond to 889 and 877 nm, respectively, and the magnitudes of their transition dipole moments are 8.0 D ($k = 0$) and 7.4 D ($k = 1$). (b, bottom) Correlation function $C_8^0 C_m^0$, which describes the coherences and the population of the β-bound pigment in cell 4, for the same realization as in Figure 3a.

and spontaneous Raman spectroscopy (ref 13, Chapter 9), but also in those cases coherences are relevant.

The second limitation is that populations are not directly measurable quantities. Even if we could do a direct measurement on single aggregates, we could still not measure the contents of Figure 3a directly. In addition true measurements are always on ensembles of systems, and the effects of homogeneous broadening cannot be incorporated in the above view.

We must realize that in a picture as shown in Figure 3a we neglect about 95% of the information available to us, by choosing just 18 populations as an indication of exciton size, rather than the 18 × 18 combinations of coefficients we could use. To demonstrate that this information is relevant, we show in Figure 3b the magnitudes of $C_8^k C_m^k$ for the same realization as was used to obtain Figure 3a. It is clear that this quantity, which represents the correlations of pigment 8 with pigments m, still extends over a large part of the ring. Even linear spectroscopic features can only be explained if we have a way to take these correlations into account.

Since the functions $F_{nv,mv'}(\omega)$ are in principle measurable quantities, it would be advantageous to find a definition of exciton length based on these correlation functions. This would in fact account for the objections given above.

In Figure 4a we plot the functions $F_{11,mv'}(\omega)$ and in Figure

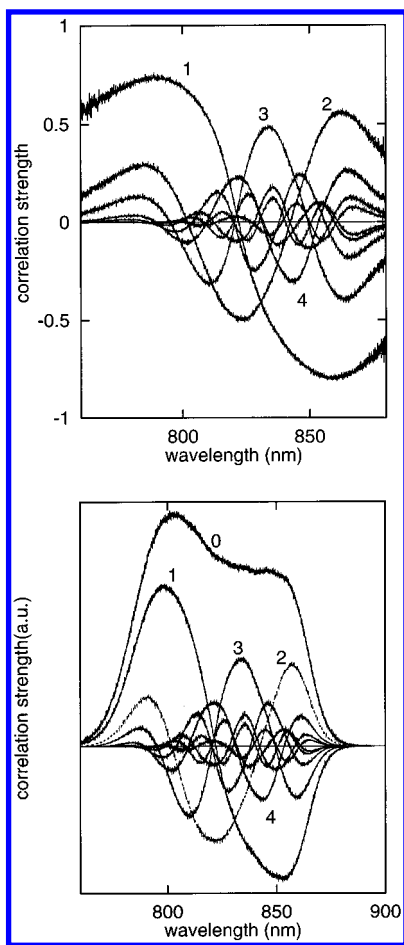**Figure 4.** (a, top) The ensemble-averaged functions, $F_{11,mv'}(\omega)$, of an α-bound BChl with its neighbors $1\beta, 2\alpha, 2\beta, ..., 5\beta$. The homogeneous line width is zero; the fwhm of the inhomogeneous distribution is 572 cm^{-1}, which corresponds to $\Delta/V \approx 1$. The curve labeled 0 is the autocorrelation function; the curves labeled 1−4 denote the first four correlation functions. (b, bottom) Relative amplitudes $F_{11,mv'}(\omega)/F_{11,11}$-($\omega$) for the same ensemble as in Figure 4a.

4b the relative amplitudes $F_{11,mv'}(\omega)/F_{11,11}(\omega)$, where the average was over a large number of realizations taken from a random distribution with width $\Delta/V \approx 2$. To get this picture we used zero homogeneous line width, to show just the effects of inhomogeneities.

Several points are immediately obvious. The original excitonic structure, described in section 2, is still present in Figure 4b. This can be seen, for instance, by comparing $F_{11,11}(\omega)$ with the envelope over the peak maxima in Figure 2 of the same function.

Next, consider the curve labeled 1 in Figure 4b. For the unperturbed ring of pigments we would get for the amplitude of $F_{11,12}(\omega)/F_{11,11}(\omega)$ at frequency ω_k using the results of the Appendix

$$\text{Re}\left[\frac{C*_{12}^{k\gamma}}{C_{11}^{k\gamma}}\right] = \cos\frac{\pi k}{N}\tan\theta(k)\cos\phi(k) \approx -\cos\frac{\pi k}{N} \quad (23)$$

This cosine-type behavior is still clearly visible in Figure 4b; only the amplitude was reduced from 1 to a lower value of approximately 0.7. Similar considerations hold for the other curves. For an ideal ring system of similar monomers all the curves should be cosines, with amplitude equal to 1. The asymmetry is caused by the fact that α- and the β-bound pigments are different and the decay in amplitudes by the overlap of excitonic states due to disorder.
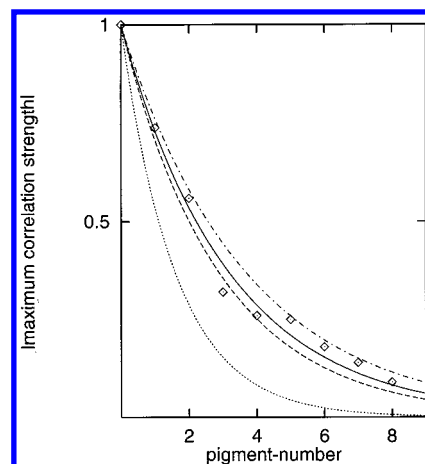

Figure 5. The maximum amplitudes ($\diamond$) of each of the scaled functions, $F_{11,mv'}(\omega)$, of Figure 4b as function of the distance between the pigments and fitted with an exponential e^{-x/x_0} (solid line). The inverse decay constant is $x_0 = 3.2$ at $\Delta = 240$ cm^{-1} and $\sigma = 0$ cm^{-1}. Also shown are the fit results for $\Delta = 240$ cm^{-1} and $\sigma = 85$ cm^{-1} (---), which results in $x_0 = 2.9$, $\Delta = 490$ cm^{-1} and $\sigma = 0$ cm^{-1} (•••), which gives $x_0 = 1.6$, and $\Delta = 0$ cm^{-1} and $\sigma = 85$ cm^{-1} ($x_0 = 3.7$) (−·−). For the last result only homogeneous broadening was used; cf. the next figure.

The relative amplitudes of the correlation function are plotted in Figure 5 and fitted with an exponential e^{-x/x_0}, which appears to give a very good fit, especially for larger values of Δ. We propose to use the decay constant x_0^{-1} of this exponent as a measure of exciton length x_0, which is thus directly related to the decay of coherences as a function of distance. In Figure 5 we show this exponential decay for various other values of Δ/V. The limiting cases discussed in the previous section also fit in nicely with this picture. For small inhomogeneous line width, smaller than the distance between the exciton levels, there is virtually no overlap between the states, and consequently there is no decay. The opposite case, a large Δ/V ratio, will lead to eq 22, and all correlations between neighboring pigments vanish.

We can now address the above objections to the original definition of exciton length. First of all there is a direct connection between spectroscopy and the value of x_0. We will consider this in detail in the next section, but at this point we would like to point out that for ordinary absorption short-range correlations are measured: owing to the ring structure the major contribution to the absorption spectrum originates from $n = 1$, 2, and 3, whereas for circular dichroism the major contribution to the spectrum comes from chromophores about a quarter of the ring apart. This is a purely geometrical effect, but it allows us, on the basis of a comparison of the spectra, to estimate the value of x_0.

In addition, although the decay is exponential, this is still much slower than the Gaussian decay the populations in Figure 3a could be fitted with. A consequence of this is that it can be understood that a large part of the ring does contribute to the CD spectrum.

One has to be careful to use these numbers directly in nonlinear spectroscopy, since the averages occurring in $\chi^{(3)}$ have in general products of four coefficients and up to three Green functions. The method given here can, however, easily be extended to nonlinear spectroscopy. Another possible extension is to use different Green functions, to model temperature-dependent behavior, or even to use time-dependent properties.

As can be inferred from eq 22 the effects of homogeneous and inhomogeneous broadening are somewhat similar. Consider a perfect ring, with only lifetime broadening. As long as the
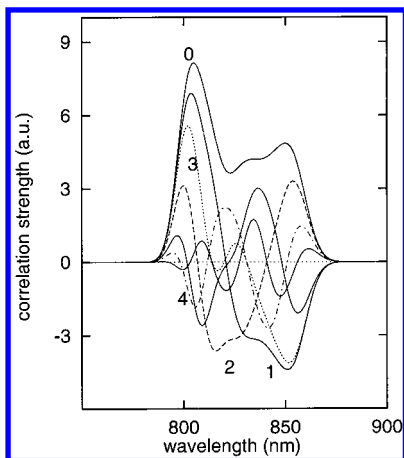
Figure 6. Coherence correlation functions, $F_{11,mv'}(\omega)$, with nv' and other numbering as in Figure 4a, for homogeneous broadening only. The width of the homogeneous distribution $\sigma = 85$ cm^{-1}, so that $\sigma/V \approx 0.4$. The decay constant in this case turns out to be $x_0 = 3.7$; cf. the previous figure.
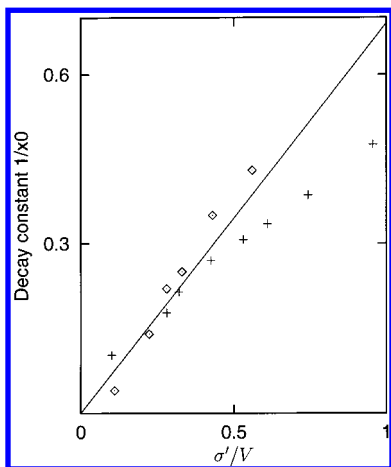

Figure 7. Decay constant x_0^{-1} as a function of the ratio σ'/V (see eq 21). Results of fits with inhomogeneous broadening only are represented by $\diamond$, those with homogeneous broadening by $+$ signs. The straight line is the curve $x_0^{-1} = 0.69 \, \sigma'/V$. For line widths larger than 0.5 σ'/V the effects of the homogeneous and the inhomogeneous broadening deviate. For *Rps. acidophila*, $V \approx 200$ cm^{-1}, and 0.5 σ'/V corresponds to a fwhm of 235 cm^{-1} in the case of homogeneous broadening and to 705 cm^{-1} for inhomogeneous broadening.

lines corresponding to individual excitonic transitions do not overlap, probing the system at a certain frequency means directly probing the excitonic level (note that not every level can be probed, since the transition dipole moment could be zero). When the lines start to overlap we probe two or more exciton levels simultaneously. This leads to cancellations, especially for the higher energy excitons, since the eigenfunctions involve more sign changes. Note that this can be viewed as localization due to phonon-coupling, since the decay-associated Green function is due to the presence of phonons in the system.[32] In Figure 6 we show the effect of just homogeneous broadening for a fwhm value of 200 cm^{-1}. There is a small decay, and consequently the "true" exciton length for the system may be slightly smaller if both homogeneous and inhomogeneous effects are taken into account.

The (apparent) exciton length x_0 for a system with a fwhm of 572 cm^{-1} for inhomogeneous and 200 cm^{-1} for homogeneous broadening is approximately 3.

In Figure 7 x_0^{-1} is plotted as a function of σ'/V. For smaller values of σ and Δ the points can be reasonably well fitted with

a straight line, as can be inferred from eq 21. For larger values that equation is no longer valid, since it was derived under the assumption that disorder does not mix eigenvalues and eigenfunctions of the exciton states. The relation between x_0 and σ'/V is well approximated by

$$\frac{1}{x_0} \approx 0.7 \frac{\sigma'}{V} \qquad (24)$$

5. Consequences of Ring Structure and Spectroscopy

The structural parts of eq 17 depend on the geometry of the ring only. We will use the B850 ring of LH2 of *Rps. acidophila* to illustrate some of the important features. It is implicitly assumed that the structure is rather rigid, even at room temperature.

In the previous section we used a one-dimensional picture to visualize the decay of the correlations functions, which is sufficient for rings of monomers. In general, for less structured assemblies a two-dimensional picture is needed;[14] in this particular case it is sufficient to distinguish between $\alpha\alpha$-, $\alpha\beta$-, and $\beta\beta$-pairs. Equation 17 gives the two possible geometric structure functions that can be used to probe the exciton manifold. For OD the last term in eq 17 can be neglected, and we are left with

$$I(w) \propto \sum_{nv,mv'} F_{nv,mv'}(\omega) \, [\vec{\mu}_{nv} \cdot \vec{\mu}_{mv'}] \equiv \mu^2 \sum_{nv,mv'} F_{nv,mv'}(\omega) \, S_{nv,mv'} \quad (25)$$

In Figure 8a the structure functions $S_{5\alpha,mv'}$ and in Figure 8b $S_{5\beta,mv'}$ are plotted for all values of mv'. In the figure the *x*-labels 9 and 10 correspond to pigments 5α and 5β (cf. section 2). The alternating behavior of these functions is a consequence of the tail-to-tail orientation of the dipole moments. We note that these functions reach their maximum values for the pigments of the same dimer: $mv' = 5\alpha$ (9) and $mv' = 5\beta$ (10) and pigments half a ring apart $mv' = 1\alpha$ (1) and $mv' = 9\beta$ (18). Since the coherence correlation functions decay exponentially, this implies that absorption spectroscopy mainly probes correlations between pigments less than a quarter of the ring apart.

The opposite is the case for circular dichroism spectroscopy. In this case we measure the difference between right and left circularly polarized light, which leads to the following expression for the rotation strength $R(\omega)$:

$$R(\omega) \propto \sum_{nv,mv'} F_{nv,mv'}(\omega) \, [\vec{\mu}_{nv} \times \vec{\mu}_{mv'}] \cdot (\vec{r}_{nv} - \vec{r}_{mv'}) \equiv \mu^2 \sum_{nv,mv'} F_{nv,mv'}(\omega) T_{nv,mv'} \quad (26)$$

Since the outer product of a vector with itself is zero, in this case the terms with equal indices do not contribute at all. In Figure 9a,b we have depicted the structure functions $T_{nv,mv'}$ for the same combinations as the absorption structure functions. Again the alternating behavior due to the arrangement of the dipole moments is observed, but now the main contribution to the CD spectrum originates from pigments further apart, where the coherence correlation functions have decayed. In principle this would allow us to give an estimate of the value of x_0 based on a comparison of the absolute magnitudes of the OD and CD spectra.

In a preceding paper,[7] we indicated that the CD spectra for degenerate pigments are small owing to canceling effects of the $\alpha\alpha$-, $\beta\beta$-, and $\alpha\beta$-contributions. Here we can further elucidate this point, using the description of LH2 in terms of
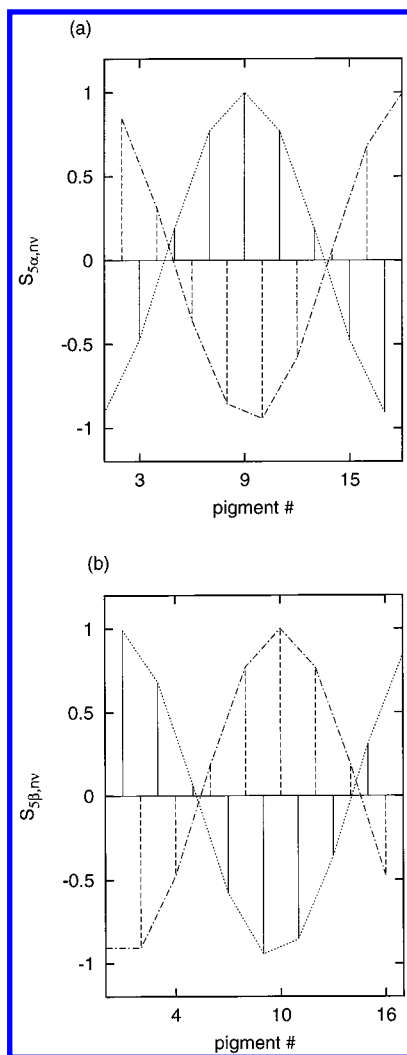
Contributions to the Linear Spectroscopy of LH2

J. Phys. Chem. B, Vol. 104, No. 18, 2000 **4497**

Figure 8. OD structure functions, $S_{5\alpha,n\nu}$ (a) and $S5_{\beta,m\nu}$ (b), for the B850 ring of LH2 of *Rps. acidophila*. There are minor differences between the two functions owing to the specific geometry of the α- and β-transition dipoles. The alternating signs are a consequence of the tail-to-tail orientation of the neighboring dipoles. The points connected by the dotted lines are those for which $\nu = \alpha$ in both figures; those connected by the dash−dotted lines are for $\nu = \beta$. These structure functions have to be multiplied with the coherence correlation functions to obtain the absorption spectrum. Since the functions displayed here have their maximum for $n\nu = m\nu'$, and for pigments half the ring apart, the autocorrelation and nearest-neighbor correlations dominate the OD spectrum. The different ways of numbering the pigments are explained in section 2.

interlocking α- and β-rings given in section 2, together with eq 26. From Figure 9 we infer that the main contribution from the individual α- and β-rings comes from pigments a half of the ring apart, where the coherence correlations are small, and in addition the sum will almost cancel. The contribution of the $\alpha\beta$-terms is largest for pigments one quarter of the ring apart, where the correlations are still appreciable, but the structure function itself has a rather low value. The $\alpha\beta$-contributions to the CD spectrum of a pigment with neighbors at its right side are opposite to the contributions with neighbors on the left. The cancellation of all contributions is almost complete for the LH2 ring of *Rps. acidophila* with the Cogdell structure and degenerate energies of the monomers ($\epsilon_\alpha = \epsilon_\beta$, cf. eq 6). This leads to a small CD and vanishing of the zero crossing of the CD spectrum in the 850 nm range.[6] There are three ways to increase the magnitude of the spectrum in this range: changing the angles that the transition dipoles of the chromophores make with the
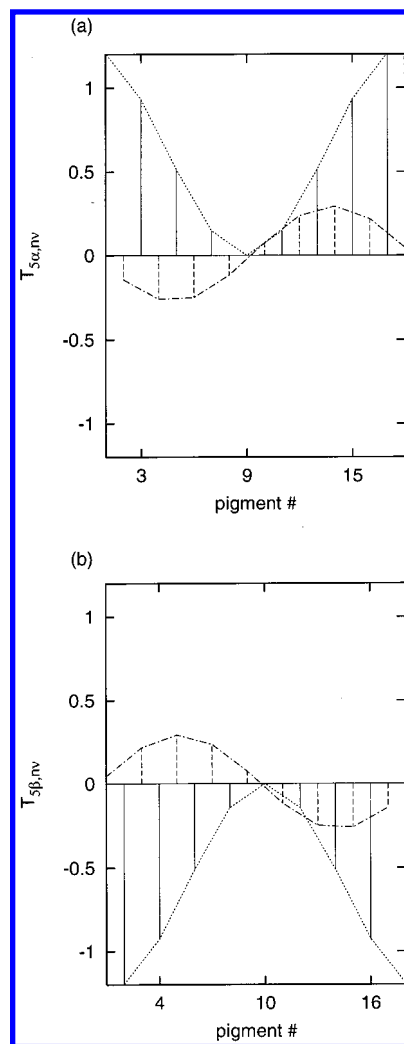

Figure 9. CD structure functions, $T_{5\alpha,m\nu}$ (a), $T_{5\beta,m\nu}$ (b), for the B850 ring in LH2 of *Rps. acidophila*. As in the previous figure in panel a the $\alpha\alpha$- and the $\alpha\beta$-combinations and in panel b the $\beta\beta$- and the $\beta\alpha$-combinations are shown. Note that these functions have the dimension of a length. These structure functions have to be multiplied with the coherence correlation functions to obtain the CD spectrum. In this case the result is zero for $n\nu = m\nu'$, and reaches a maximum for pigments a quarter of the ring apart. Therefore longer range correlations determine the CD spectrum. Note, however, that the $\alpha\beta$- and $\beta\alpha$-combinations probe the correlation functions with a different sign, and so do the $\alpha\beta$- and $\beta\alpha$-combinations. As a result CD practically vanishes for the B850 ring. This point is further elucidated in Figure 12.

plane of the ring or with the tangent of the ring. Both reduce the cancellation effects for geometric reasons. The third possibility is lifting the degeneracy of the monomers, which changes the coherence correlation functions with similar results. Some of the consequences of these changes and their relative effects were also discussed in refs 7 and 11. We note that changes in the orientations of the dipole moments largely conserve the excitonic correlations; the interaction energies do not change much, but they do change the geometric structure factors. Changes in the sites energies, however, affect the excitonic correlations only, whereas the geometric structure factors remain unaltered.

In the remainder of this section we show how the coherence correlation functions combine with the geometric structures to give the spectra. We look at two cases in particular, one where the excitation energies of the monomers are the same and one where they differ by the amount necessary to obtain a reasonable CD spectrum. In both cases the inhomogeneous line width is Δ
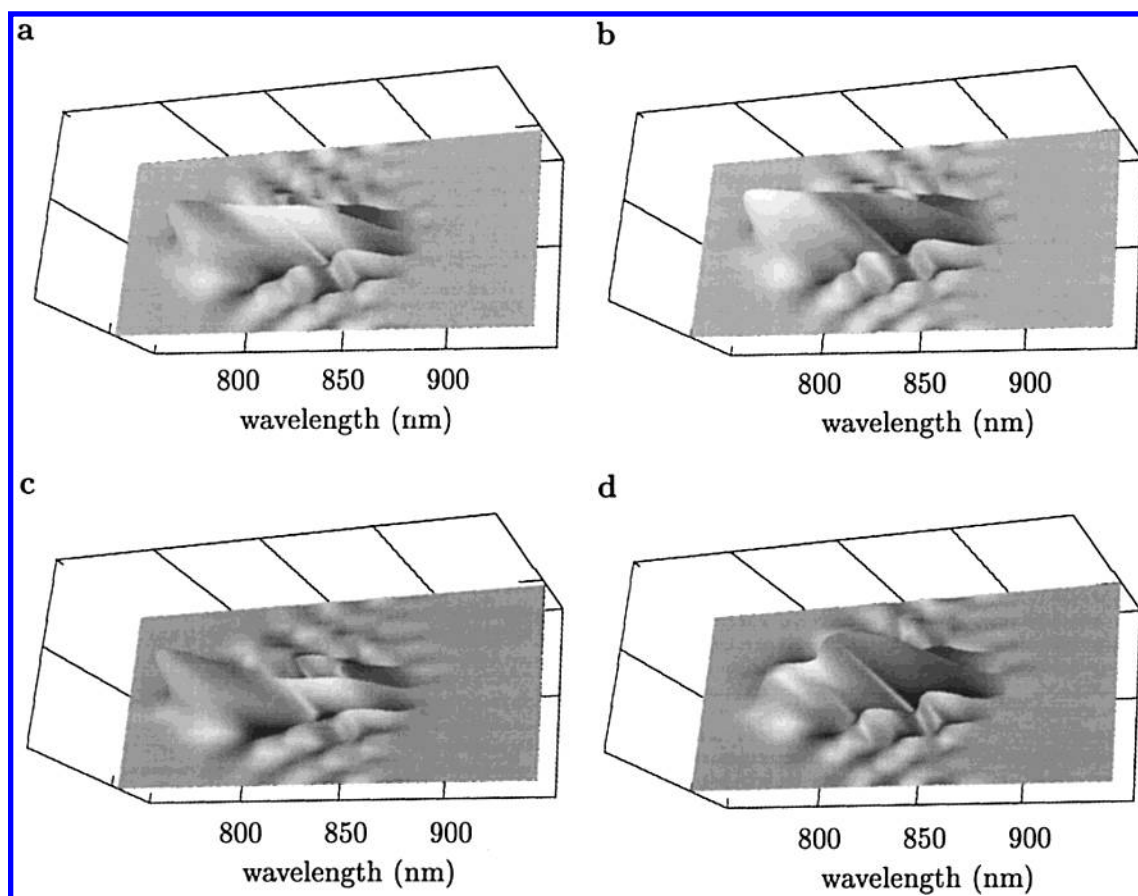
Figure 10. (a, c) Correlation functions $\mathcal{F}_{5\alpha,m\nu'}(\omega)$ of an α-bound BChl shown as a function of the wavelength, for $m\nu'$ ranging over all B850 pigments. (b, d) Correlation functions $\mathcal{F}_{5\alpha,m\nu}(\omega)$ with a β-bound BChl. The α- and the β-bound BChl's are degenerate in the cases a and b. In the panels c and d the same functions are shown for nondegenerate dimers; the energy difference between the α- and the β-bound BChl's is 300 cm^{-1}. For the α -bound BChl's we chose 12 300 cm^{-1} (813 nm), and for the β-pigments 12 000 cm^{-1} (833 nm) was used. In all panels, the wavelength scale (the long x-axis) ranges from 750 to 950 nm. The short y-axis identifies $m\nu$. The tick mark indicates BChl 5α, the position of the autocorrelation in the panels b and d. At the short-wavelength side, the functions are positive for all $m\nu'$, and at the longer wavelengths the signs alternate. The profiles of figures and the intensities are very similar in panels a and b, as are the positions of the maxima. These positions differ with the wavelengths at which the maxima occur in panels c or d. On the short-wavelength side the correlations decay much faster than on the red side. The autocorrelation of an α-bound BChl is strongest at shorter wavelengths, and the β-bound BChl's have their strongest contribution at the long-wavelength side. Decreasing the energy of the β-bound pigments has a pronounced effect on the correlation functions at the red edge of the energy spectrum.

= 240 cm^{-1}, corresponding to a fwhm of 570 cm^{-1}, and the homogeneous line width is $\sigma = 85$ cm^{-1}, corresponding to a fwhm of 200 cm^{-1}. Since the nearest-neighbor interaction is approximately $V = 200$ cm^{-1}, this leads to considerable overlap of the excitonic states, and Figure 7 of the previous section applies. The monomer energy is chosen to be 12 150 cm^{-1} (823 nm) to yield spectral features in the right wavelength region.

In Figure 10a,b we show the coherence correlation functions $\mathcal{F}_{5\alpha,m\nu'}(\omega)$ ($m = 1, ..., 9, \nu' = \alpha, \beta$) and $\mathcal{F}_{5\beta,m\nu'}(\omega)$ ($m = 1, ..., 9, \nu' = \alpha, \beta$). In the Figure 10c,d we show the same functions but now for a static energy mismatch of 300 cm^{-1}. For the α-monomers we chose 12 300 cm^{-1} (813 nm), and for the β-pigments 12 000 cm^{-1} (833 nm) was used. The nearest-neighbor correlation is negative at the long-wavelength side and positive at the blue side. The excitonic patterns are also very clear for the next-nearest neighbors and so forth. The overlap of the lines, due the line broadening mechanisms, results in the decay of the correlations between pigments far apart.

The combination of Figures 8 or 9 and Figure 10 yields the contributions of the pigments to the spectra as a function of the wavllength. In Figure 11 these are shown in the case of nondegenerate site energies of α- and β-bound pigments. The energy mismatch is taken equal to 300 cm^{-1} as in Figure 10c,d. We notice that indeed the OD spectrum has contributions mainly from the center ("populations") and drops off rapidly, whereas

CD gets positive and negative contributions from all coherences. The OD and CD spectra are obtained by summing all contributions for each wavelength. The resulting spectra are shown in Figure 12 for both degenerate and nondegenerate α- and β-bound pigments.

The CD spectrum depends on the difference between the αα- and the ββ-contributions; contributions to the CD of α-pigments only are opposite to the ββ-combinations, changes in the site energies change the ratio of these contributions at the red side of the spectrum, as was discussed previously. The CD arising from αβ-combinations is very small and identical in both cases. A linear dichroism experiment with all LH2's in the xy-plane, and the incident light polarized along the z-axis, yields a signal proportional to the z-components of the transition moments.[39,40] The structure function corresponding to LD is particularly simple since the z-components of the chromophores in the B850 ring of *Rps. acidophila* all have equal sign and almost equal magnitude. This means that the LD spectrum of *Rps. acidophila* depends directly on the correlations. At the ends of the spectrum the αα- and the ββ-correlations are all positive. The αβ-correlation cancels the autocorrelations in the red part and enhances them in the blue. This leads to relatively strong LD features in the 800 nm region and very weak contributions at the very red edge of the 850 band.
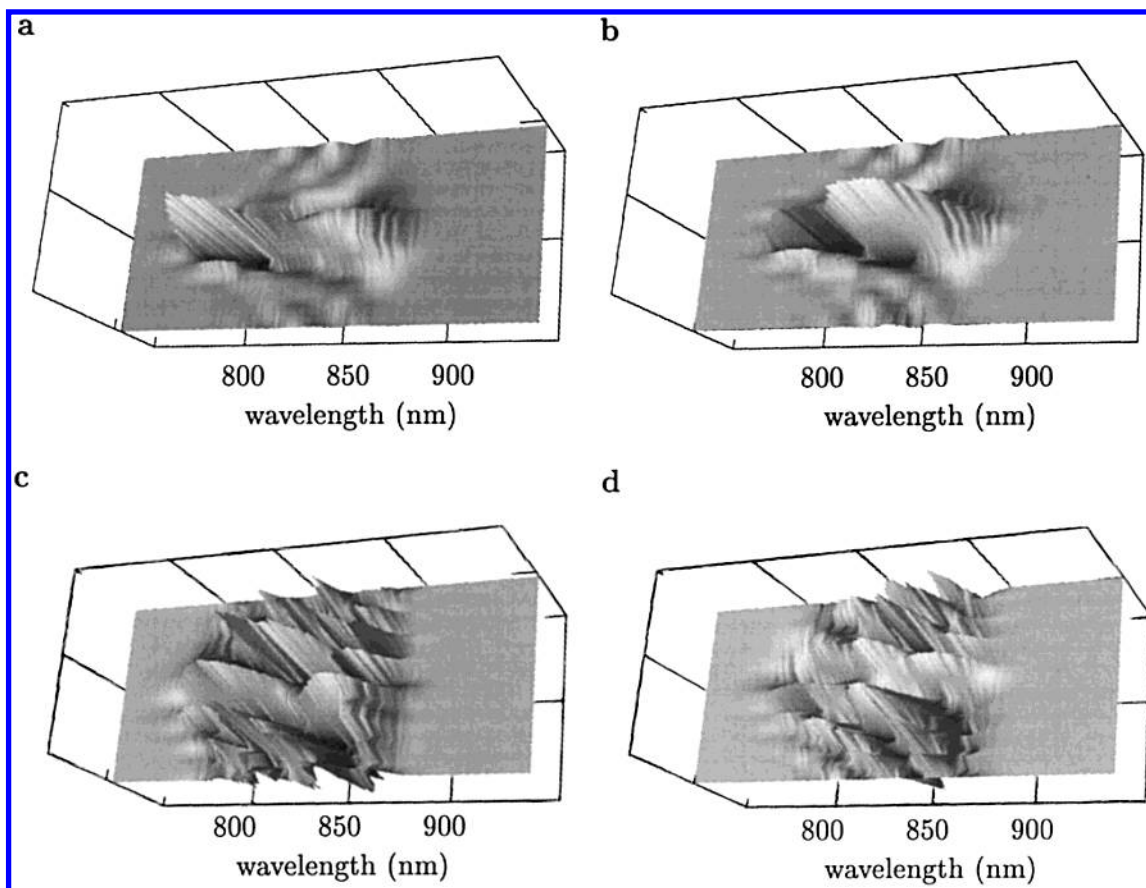
Contributions to the Linear Spectroscopy of LH2

J. Phys. Chem. B, Vol. 104, No. 18, 2000 **4499**

Figure 11. Functions $F_{5\alpha,mv'}(\omega)$ and $F_{5\beta,mv'}(\omega)$ multiplied by the OD structure function (a, b) and multiplied with CD structure function (c, d). See the caption of Figure 10 for the description of the axes. The energy difference between the α- and the β-bound BChl's is 300 cm^{-1} in this figure. Panels a and b show how the signs alternate at the short-wavelength while all correlations are positive at longer wavelengths. The main contribution to the absorption arises from the nearest neighbors as is clearly seen in panels a and b. The CD products in panels c and d, however, hardly show any decrease in intensity for BChl's further apart; the autocorrelation function is of course zero for all values of ω. The correlation functions decrease for pigments further apart, but the structure functions become larger, see Figure 9. For every ω the signs of the product functions now alternate as a function of mv'.

6. "Typical Cases" and Relation to Other Measures of Exciton Length

Recently another measure of the correlation length was introduced by Chachisvilis,[41] and a similar measure was also used by Monshouwer.[42] Its definition can in our notation be written as

$$C(n) = \langle C_1^0 \, C_{1+n}^0 \rangle \qquad (27)$$

where the distinction between α and β was neglected.

Thus the average is over the lowest excitonic state, regardless of its energy. In this connection, typical cases are sometimes also invoked, which purport to describe the behavior of these lowest energy excited states.

Typical correlation lengths resulting from this definition are usually also in the range 3−5, which is not entirely surprising since the main contribution to this correlation function originates of course also from states close to the average energy of the lowest energy state. This can be shown more clearly by considering the function

$$F_{nm}^{\theta}(\omega) = \langle \theta(\omega - \omega_0) \, C_n^0 \, C_m^0 \rangle \qquad (28)$$

where the ensemble average is now over the lowest excitonic only. This result would then have to be contracted with $\vec{\mu}_n \cdot \vec{\mu}_m$ to describe the superradiance measurements by Monshouwer.[42]

It is obvious that the short-range correlations are favored in these measurements, as with regular absorption.

In this context it is illustrative to look at some so-called typical cases. In Figure 13 we show two typical cases picked from the random distributions discussed in the previous section. First of all, only states at the extreme red edge of the excitonic band give the "typical" picture of the very rapidly decaying populations depicted in Figure 3a, and even in those cases the correlations between the pigments cannot be neglected. For states that are taken more from the center of the distribution, coherences and populations appear to extend over a larger part of the ring and are indistinguishable from realizations of higher excitonic states.

Another measure that is frequently used is the participation ratio, defined by its inverse: the number of coherent pigments at energy ω,[43,44] which in our notation would be proportional to

$$\left\langle \sum_k \delta(\omega - \omega_k) \sum_n |C_n^k|^4 \right\rangle \qquad (29)$$

This is again a population measure: only states with the same n (same pigment) contribute to this quantity, and as such it is only relevant in selected nonlinear optical experiments, namely, those in which coherences do not play a role. To use it for linear optical experiments would be wrong. For instance it severely underestimates the participation of pigments in CD experiments.
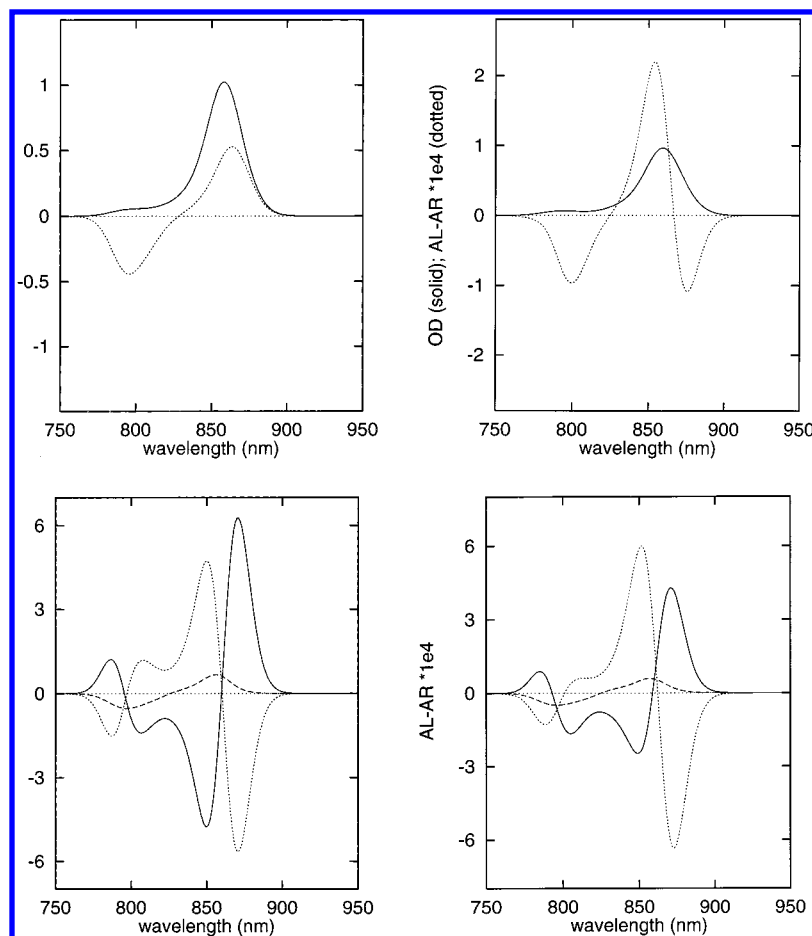
Figure 12. (a, top right and b, top left) OD (solid lines) and CD (dotted lines) spectra. (c, bottom left and d, bottom right) Contributions to the CD spectra of the ring of α-BChl's only (solid), of β-bound BChl's only (dotted), and the CD arising from the combination of these rings, αβ (dashed). The sum of these yields the CD spectrum. In panels a and c the BChl's in the dimer are degenerate, and in panels b and d their energy difference equals 300 cm^{-1}. Panel c shows that the CD arising from the ring of α-bound BChl's cancels the CD of the β-bound BChl's, a consequence of the properties of the structure functions shown in Figure 9. The total signal is rather similar to the CD of the αβ-combination; it is small and does not show a zero crossing in the 860 nm region. Panel d shows that lifting of the degeneracy amplifies the CD of the β ring at the long-wavelength side of the spectrum, so that it is no longer canceled by the contribution of the α-ring.

In addition the values depend on the choice of basis for degenerate systems. As was pointed out by Monshouwer,[24] different authors find different coherence sizes for the same system, only by choosing a different basis set of excitonic functions.

7. Remarks and Conclusions

This paper presented analysis of the absorption and the CD spectra in terms of a real space description and is particularly successful since the effects of the excitonic structure of the B850 ring on one hand and the effects of the structure of the complex in combination with the experimental probe on the other hand are separated. Effects on the CD and OD spectra due to changes in geometry of the system are very easily understood as well as the effect of the energy mismatch between the α- and the β-bound BChls. Furthermore, on the basis of this model detailed insight is gained of the averaged excitonic structure of the complex. The real space description of the averaged density matrix still exhibits the ninefold symmetry, indicating equal excitation probability. As a result of the line-broadening mechanisms, the coherences in the density matrix decay exponentially. These coherences describe the correlations between the pigments and determine the frequency behavior of the complex. Spectra can then be understood as the result of probing these correlation functions with different types of

probes. Thus we found that with OD mainly short-range correlations are probed, whereas CD probes longer ranged correlations.

A definition of the exciton length based on the decay behavior of the correlation functions relates the spectroscopic properties to the excitonic properties of the system. Therefore we suggest a concurrent definition of the exciton length based on the steepness of the exponent, which describes the decay of the correlation functions in space due to line-broadening mechanisms. In this way the exciton length and the spectroscopic features of the system are well defined for localized and delocalized excitons.

For the cases studied here the correlation length (exciton length) as defined by the decay of coherence correlation functions is independent of the frequency, and for the parameters used in the calculations is approximately equal to three. This is not necessarily true. Only when all excitonic lines overlap considerably is this the case. The width of the exciton manifold is mainly determined by the nearest-neighbor interaction, but the distance between the excitonic lines is much smaller at the edges of the manifold than in the middle. This means that for smaller homogeneous/inhomogeneous line width we can see spatial decay of the correlation functions for the extremal
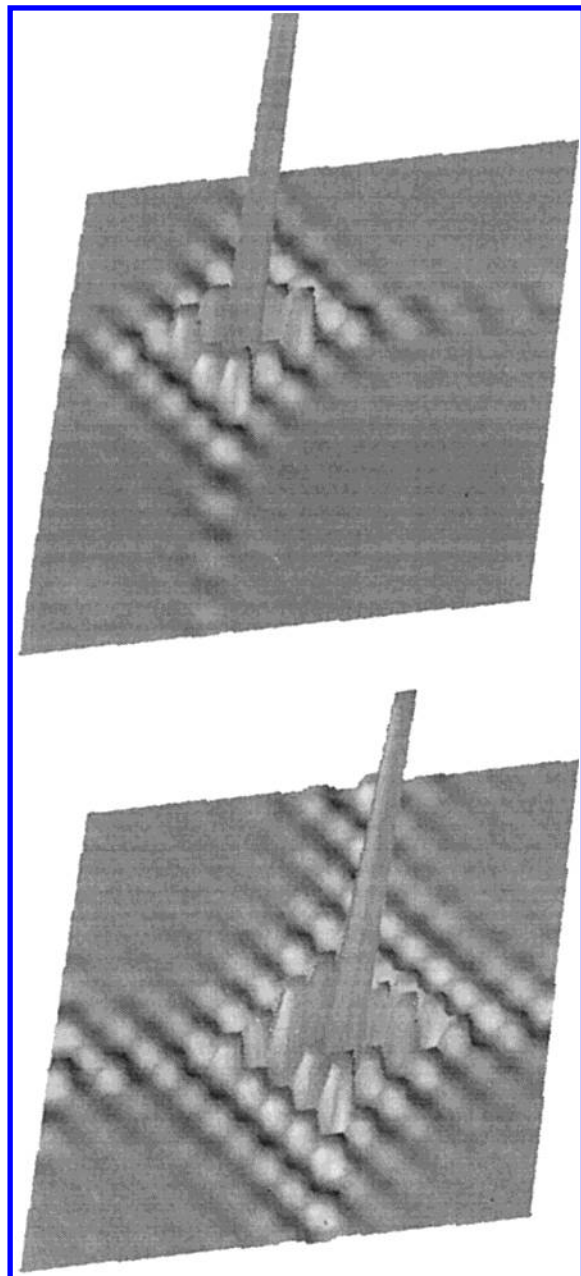
Contributions to the Linear Spectroscopy of LH2

J. Phys. Chem. B, Vol. 104, No. 18, 2000 **4501**

Figure 13. Correlation functions, $F_{nm}^{\theta}(\omega)$, see eq 28, belonging to the lowest exciton band of one realization picked from a Monte Carlo simulation of 10.000 runs. The selection of the realization is based on the frequency of the lowest transition. The fwhm of the energy distribution is 572 cm^{-1}, and the energy difference between the α- and the β-bound BChl's is 300 cm^{-1}. In panel a the frequency is found in the interval $10\,000 < \omega(k=1) < 11\,000$ cm^{-1}, which corresponds to $909-917$ nm. In panel b the frequency of the lowest level is $11\,450 < \omega(k=0) < 11\,550$ cm^{-1}, i.e., $866-873$ nm. The probability of finding the lowest exciton function in a specific interval is smaller for the frequency intervals further away from the smallest transition frequency in the system without energetic disorder. The probabilities for finding an energy in the intervals are 0.3% in panel a (top) and 34% in panel b (bottom), respectively.

frequencies, but not for frequencies related to energies in the middle of the manifold. An example of this is given in Figure 2a,b.

The value of $\Delta/V \approx 1-2$ used in this paper to model the correlation function and spectra gives good agreement with observed line widths at room temperature.[7,11] Similar values were also used by refs 24 and 42 to model superradiance experiments. An recent indirect confirmation comes from single-

molecule experiments,[47] where the observed inhomogeneity is consistent with a delocalization over $4-5$ pigments and a Δ/V value of approximately 2. This is in contrast to the results by Small and co-workers,[35,37] who on the basis of hole-burning experiments find smaller values for the disorder, and consequently a larger exciton length, and less oscillation strength in the lowest excitonic level.

We also note that the calculation of the unperturbed (or average) excitonic states is still useful for understanding the features of the averaged exciton correlation functions. The averages reflect the ninefold symmetry of the unperturbed system; only the amplitudes of the correlation functions have decayed.

For the model used here homogeneous and inhomogeneous broadening have similar effects. The reason is that we have assumed the same homogeneous line width for each of the excitonic lines of every realization of a disordered system. This means that we can either give each line of a realization a homogeneous lined width, thus speeding up the MC calculation by several orders of magnitude, or at the end of the calculation convolute the inhomogeneously broadened correlation function with the homogeneous Gaussian. Equation 15 can also be written as

$$F_{nv,mv'}(\omega) = \frac{1}{\sqrt{2\pi}\sigma} \int_{-\infty}^{\infty} d\omega'\, e^{-(\omega-\omega')^2/2\sigma^2} \sum_k \langle \delta(\omega' - \omega_k)\, C_{nv}^k\, C_{mv'}^k \rangle \quad (30)$$

which is a much slower procedure.

In general, however, the functions $G(\omega_0 - \omega_k)$ are not the same for each level. Obviously it is easy within the context of the model presented in this paper to include a different homogeneous line width for each level in every realization. A common approach is to assume that the lowest excitonic level has a much longer lifetime than the other levels and that within a very short time an excited-state Boltzmann distribution pertains.[45] These considerations do not play a major role in regular absorption and CD spectroscopy, although it is possible to get a better fit of the red edge of the B850 CD spectrum using a smaller lowest exciton line width, but they are extremely relevant in, for instance, fluorescence decay and other nonlinear forms of spectroscopy.

The Green functions, $G(\omega_0 - \omega_k)$, reflect the time-dependent properties of the system. Implicit for the model used here is that localized states, that is, states where the excitation is localized on one or more pigments, do not remain localized. For the homogeneous and inhomogeneous broadening parameters used, decay and delocalization takes place within about 50 fs. This can be shown directly by Fourier transformation of the functions $F_{nm}(\omega)$. We note that the similarity of Figures 4a and 6 will lead to similar behavior in time of the correlation functions, even though the underlying mechanisms are completely different. It is not possible to directly access this behavior experimentally.

To give an adequate description of the dynamics of excitation transfer, and from there to the Green functions, we would need a consistent model for the relaxation and transfer mechanisms among the excitonic levels, and between excitonic levels and the ground state. This is beyond the scope of this paper.

Appendix. Solution of the Dimer Problem

The full solution of the dimer problem was already given in Appendix C of ref 46 and will not be repeated here; we just give the results in terms of the quantities introduced in section 2. Equation 8 shows that we have to solve the following eigenvalue problem for every value of k:

$$\mathcal{H}|\psi_k, 1\rangle = (\epsilon_1 + \tilde{V}_{11}(k)) |\psi_k, 1\rangle + \tilde{V}_{21}(k) |\psi_k, 2\rangle \quad (A1)$$

$$\mathcal{H}|\psi_k, 2\rangle = (\epsilon_2 + \tilde{V}_{22}(k)) |\psi_k, 2\rangle + \tilde{V}_{12}(k) |\psi_k, 1\rangle \quad (A2)$$

For this problem the eigenvalues are

$$\epsilon_{1,2}(k) = \frac{1}{2}(\epsilon_1 + \tilde{V}_{11}(k) + \epsilon_2 + \tilde{V}_{22}(k)) \pm$$
$$\frac{1}{2}\sqrt{(\epsilon_1 + \tilde{V}_{11}(k) - \epsilon_2 - \tilde{V}_{22}(k))^2 + 4|\tilde{V}_{21}(k)|^2} \quad (A3)$$

and the eigenfunctions can be written as

$$|\epsilon_1(k)\rangle = \cos\theta(k) |\psi_k, 1\rangle + \sin\theta(k)e^{i\phi(k)}|\psi_k, 2\rangle \quad (A4)$$

and

$$|\epsilon_2(k)\rangle = -\sin\theta(k)e^{-i\phi(k)} |\psi_k, 1\rangle + \cos\theta(k) |\psi_k, 2\rangle \quad (A5)$$

with

$$\tan\theta(k) = \frac{\epsilon_1(k) - \epsilon_1 - \tilde{V}_{11}(k)}{|\tilde{V}_{21}(k)|} \quad (A6)$$

and

$$\epsilon^{i\phi(k)} \tilde{V}_{12}(k) = |\tilde{V}_{12}(k)| \quad (A7)$$

These results can be summarized as

$$|\epsilon_\gamma(k)\rangle = \sum_{\nu=1}^{2} \sum_{n=1}^{N} C_{n\nu}^{k\gamma} |n, \nu\rangle \quad (A8)$$

where the coefficients $C_{n\nu}^{k\gamma}$ can be found from eqs A4 and A5 together with eq 7. Thus, for instance

$$C_{n1}^{k1} = \frac{1}{\sqrt{N}} e^{2\pi ikn/N} \cos\theta(k)$$

References and Notes

(1) van Grondelle, R.; Dekker, J. P.; Gillbro, T.; Sundström, V. *Biochim. Biophys. Acta* **1994**, *1187*, 1.

(2) Sundström, V.; Pullerits, T.; van Grondelle, R. *J. Phys. Chem. B* **1999**, *103*, 2327.

(3) McDermott, G.; Prince, S. M.; Freer, A. A.; Hawthornthwaite-Lawless, A. M.; Papiz, M. Z.; Cogdell, R. J.; Isaacs, N. W. *Nature* **1995**, *374*, 517.

(4) Pullerits T.; Sundström, V. *Acc. Chem. Res*. **1996**, *29*, 381.

(5) Fleming, G. R.; van Grondelle, R. *Curr. Opin. Struct. Biol*. **1997**, *7*, 738.

(6) Sauer, K.; Cogdell, R. J.; Prince, S. M.; Freer, A. A.; Isaacs, N. W.; Scheer, H. *Photochem. Photobiol*. **1996**, *64*, 564.

(7) Koolhaas, M. H. C.; van der Zwan, G.; Frese, R. N.; van Grondelle, R. *J. Phys. Chem. B* **1997**, *101*, 7262.

(8) Alden, R. G.; Johnson, E.; Nagarajan, V.; Parson, W. W.; Law, C. J.; Cogdell, R. J. *J. Phys. Chem. B* **1997**, *101*, 4667.

(9) Fowler, G. J. S.; Sockalingum, G. D.; Robert, B.; Hunter, C. N. *Biochemistry* **1994**, *299*, 695.

(10) Fowler, G. J. S.; Visschers, R. W.; Grief, G. G.; van Grondelle, R.; Hunter, C. N. *Nature* **1992**, *355*, 848.

(11) Koolhaas, M. H. C.; Frese, R. N.; Fowler, G. J. S.; Bibby, T. S.; Georgakopoulou, S.; van der Zwan, G.; Hunter, C. N.; van Grondelle, R. *Biochemistry* **1997**, *37*, 4693.

(12) Liuolia, V.; Valkunas, L.; van Grondelle, R. *J. Phys. Chem. B* **1997**, *101*, 7343.

(13) Mukamel, S. *Principles of Nonlinear Optical Spectroscopy*; Oxford University Press: New York, 1995.

(14) Wagersreiter, T.; Mukamel, S. *J. Chem. Phys*. **1996**, *104*, 7086.

(15) Koolhaas, M. H. C. Thesis, Vrije Universiteit, Amsterdam, 1998.

(16) Somsen, O. J. G.; van Grondelle, R.; van Amerongen, H. *Biophys. J*. **1995**, *71*, 1934.

(17) van Mourik, F.; Visschers, R. W.; Chang, M. C.; Cogdell, R. J.; Sundström, V.; van Grondelle, R. In *Membrane Bound Complexes in Phototrophic Bacteria*; Drews, G.; Dawes, E. A., Eds.; Plenum Press: New York, 1990; pp 435−456.

(18) Visser, H. M.; Somsen, O. J. G.; van Mourik, F.; Lin, S.; van Stokkum, I. H. M.; van Grondelle, R. *Biophys. J*. **1995**, *69*, 1083.

(19) Novoderezhkin, V. I.; Razjivin, A. P. *FEBS Lett*. **1995**, *368*, 370.

(20) Sauer, K. *Biophys. J*. **1996**, *59*, A−23.

(21) Sturgis, J. N.; Robert, B. *Photosynth. Res*. **1996**, *50*, 5.

(22) Jimenez, R.; Dikshit, S. N.; Bradforth, S. E.; Fleming, G. R. *J. Phys. Chem*. **1996**, *100*, 6825.

(23) Pullerits, T.; Chachisvilis, M.; Sundström, V. *J. Phys. Chem*. **1996**, *100*, 10787.

(24) Monshouwer, R.; van Grondelle, R. *Biochim. Biophys. Acta* **1996**, *1275*, 70.

(25) Leupold, D.; Stiel, H.; Teuchner, K.; Nowak, F.; Sandner, W.; Ücker, B.; Scheer, H. *Phys. Rev. Lett*. **1996**, *77*, 4675.

(26) Bopp, M. A.; Jia, Y. W.; Li, L. Q.; Cogdell, R. J.; Hochstrasser, R. M. *Proc. Natl. Acad. Sci. U.S.A*. **1997**, *94*, 10630.

(27) Kumble, R.; Palese, S.; Visschers, R. W.; Dutton, P. L.; Hochstrasser, R. M. *Chem. Phys. Lett*. **1996**, *261*, 396.

(28) Bradforth, S. E.; Jimenez, R.; van Mourik, F.; van Grondelle, R.; Fleming, G. R. *J. Phys. Chem*. **1995**, *99*, 16179.

(29) Jimenez, R.; van Mourik, F.; Yu, J. Y.; Fleming, G. R. *J. Phys. Chem. B* **1997**, *101*, 7350.

(30) Yu, J.-Y.; Nagasawa, Y.; van Grondelle, R.; Fleming, G. R. *Chem. Phys. Lett*. **1997**, *280*, 404.

(31) Fidder, H. Thesis, Rijksuniversiteit Groningen, Groningen, 1993.

(32) Leegwater, J. A. *J. Phys. Chem*. **1995**, *99*, 11605.

(33) Karrasch, S.; Bullough, P.; Ghosh, R. *EMBO*. **1995**, *14*, 631.

(34) Kramer, H. J. M.; Pennoyer, J. D.; van Grondelle, R.; Westerhuis, H. W. J.; Niederman, R. A.; Amesz, J. *Biochim. Biophys. Acta* **1984**, *767*, 335.

(35) Wu H.-M.; Small, G. J. *Chem. Phys*. **1997**, *218*, 225.

(36) Hecht, E. *Optics*, 2nd ed.; Addison-Wesley Publishing Company: Reading, MA, 1990.

(37) Wu, H. M.; Reddy, N. R. S.; Small, G. J. *J. Phys. Chem. B* **1997**, *101*, 651.

(38) Nagarajan, V.; Alden, R. G.; Williams, J. C.; Parson, W. W. *Proc. Natl. Acad. Sci. U.S.A*. **1996**, *93*, 13774.

(39) Wendling, M.; Monshouwer, R.; van Grondelle, R. Manuscript in preparation.

(40) Cantor, C. R.; Schimmel, P. *Biophysical Chemistry*; W. H. Freeman and Company: New York, 1980.

(41) Chachisvilis, M.; Kühn, O.; Pullerits, T.; Sundström, V. *J. Phys. Chem. B* **1997**, *101*, 7275.

(42) Monshouwer, R.; Abrahamson, M.; van Mourik, F.; van Grondelle, R. *J. Phys. Chem. B* **1997**, *101*, 7241.

(43) Fidder, H.; Knoester, J.; Wiersma, D. A. *J. Chem. Phys*. **1991**, *95*, 7880.

(44) Schreiber, M.; Toyozawa, Y. *J. Phys. Soc. Jpn*. **1982**, *51*, 1528.

(45) Monshouwer, R.; Baltuška, R.; van Mourik, F.; van Grondelle, R. *J. Phys. Chem*. **1998**, *102*, 4360.

(46) Koolhaas, M. H. C.; van der Zwan, G.; van Mourik, F.; van Grondelle, R. *Biophys. J*. **1996**, *72*, 1828.

(47) van Oijen, A. M.; Ketelaars, M.; Köhler, J.; Aartsma, T. J.; Schmidt, J. *Science* **1999**, 400.